

Multimodal transition and excitability of a neural oscillator

L. S. Borkowski

Department of Physics, Adam Mickiewicz University, Umultowska 85, 61-614 Poznan, Poland

We analyze the response of the Morris-Lecar model to a periodic train of short current pulses in the period-amplitude plane. For a wide parameter range encompassing both class 2 and class 3 behavior in Hodgkin's classification there is a multimodal transition between the set of odd modes and the set of all modes. It is located between the 2:1 and 3:1 locked-in regions. It is the same dynamic instability as the one discovered earlier in the Hodgkin-Huxley model and observed experimentally in squid giant axons. It appears simultaneously with the bistability of the states 2:1 and 3:1 in the perithreshold regime. These results imply that the multimodal transition may be a universal property of resonant neurons.

PACS numbers: 87.19.lb,87.19.1l,87.19.ln

I. INTRODUCTION

In 1948 Hodgkin studied the response of neurons to stimulation by a constant current [1]. He summarized his findings by dividing neurons into three classes: those having continuous relation between the current amplitude and response frequency (type 1), those with a discontinuous jump of response frequency at the stimulus threshold (type 2), and those which spike only once or twice to the constant current stimulus (type 3). It is now a widely accepted view that integrator (resonator) neurons exhibit type 1 (type 2) behavior, respectively. Well known examples of type 2 neurons include Hodgkin-Huxley (HH) [2], fast-spiking cortical cells [3, 4], Morris-Lecar (ML) [5, 6] and Hindmarsh-Rose [7] models. Some neuron models are known to exhibit different types of excitability, depending on parameter values. Prescott et al. [8] showed in the ML model, originally used to describe the barnacle giant muscle fiber, that change of one parameter was sufficient to switch between type 1, type 2, and type 3 dynamics. Mathematically speaking, class 1 excitability occurs through a saddle-node bifurcation, class 2 excitability occurs through a Hopf bifurcation, and class 3 excitability is a result of a quasiseparatrix crossing. The ML model consists of equations describing the time evolution of two dynamic variables, the fast and the slow one. Prescott et al. [8] emphasized that the change of excitability in this system was a result of competition between slow and fast currents. The ML model was also used as a minimal model in the investigation of changes of the dynamics of the CA1 pyramidal neurons between type 1 and type 2 [9].

There is more evidence that the spike initiation mechanism is not a fixed property of the neuron. In some experiments the squid giant axons had type 3 instead of type 2 excitability [10, 11]. The discrepancy between the type 2 behavior of the HH model and experiment was explained by modifying a single parameter in the term describing the potassium current [12]. In a recent study of the periodically stimulated HH model by the present author it was found that the firing rate may be either continuous or discontinuous function of the current ampli-

tude, depending on the stimulus frequency [13]. Bistable behavior at the excitation threshold was identified as a signature of an antiresonant regime of a resonant neuron. When brief stimuli arrive at resonant frequencies, the HH neuron may respond with arbitrarily low firing rate. The dependence of the firing rate on the current amplitude scales with a square root above the threshold, consistent with a saddle-node bifurcation [14].

The HH neuron's response at resonant frequencies can be divided into three regimes: (i) short pulses, where the width τ does not exceed the optimal width τ_{opt} associated with a minimum threshold τ_{opt} , (ii) $\tau_{opt} < \tau < T_{res}$, and $\tau \simeq T_{res}$ [13]. The Hodgkin classification scheme is related to case (iii). The analysis of response in the limit of short stimuli gives a much more interesting information about the neuron's dynamics [13]. Since the behavior of the HH model at the threshold depends on stimulation frequency, it would be useful to investigate the same problem in a simpler neural oscillator, such as the ML model, which can be viewed as a minimal model of a resonant neuron.

An important question related to the study of excitability is the existence of the dynamic singularity in the ML model. The recently discovered multimodal transition (MMT) [15] in the response of the HH cells at frequencies above the main resonant frequency manifests itself as a change of the parity of response modes, strongly affecting the dynamics in its vicinity. Experimental data of Takahashi et al. [16] provide strong evidence for the existence of this transition [17]. The MMT occurs just above the threshold, between the locked-in states 2:1 and 3:1. Could this be a universal property of resonant neurons? How does the MMT relate to the Hodgkin's classification?

The knowledge of the perithreshold behavior of various groups of neurons is crucial if we want to understand their role in encoding different types of neural input [3, 4, 18, 19]. There is also another important reason for studying patterns of excitability. Finding regimes of similar behavior in different models would provide justification for replacing more complex sets of equations by simpler ones. For example, we can ask under what circumstances the ML model, or its equivalent, could be

used as a reasonable simplification of the HH-type models. It was shown earlier that the relaxation times of both the HH model and the type 2 version of the ML model just below the threshold of repetitive firing, when stimulated by a constant current, were both equal to $1/2$ [20]. Does this similarity extend to finite stimulus frequencies?

II. THE MODEL AND RESULTS

We use the form of the ML model proposed by Prescott et al. [8],

$$C \frac{dV}{dt} = -g_{fast} m_{\infty}(V)(V - E_{Na}) \quad (1)$$

$$- g_{slow} w(V - E_K) - g_L(V - E_L) + I_{app}, \quad (2)$$

$$dw/dt = \phi_w \frac{w_{\infty}(V) - w}{\tau_w(V)}, \quad (3)$$

$$m_{\infty}(V) = 0.5 \left[1 + \tanh \left(\frac{V - \beta_m}{\gamma_m} \right) \right], \quad (4)$$

$$w_{\infty}(V) = 0.5 \left[1 + \tanh \left(\frac{V - \beta_w}{\gamma_w} \right) \right], \quad (5)$$

$$\tau_w(V) = 1 / \cosh \left(\frac{V - \beta_w}{2\gamma_w} \right). \quad (6)$$

The fast activation variable V competes with the slow recovery variable w . Parameter values were chosen in Ref. [8] to produce different spiking patterns: $E_{Na} = 50\text{mV}$, $E_K = -100\text{mV}$, $E_L = -70\text{mV}$, $g_{fast} = 20\text{mS/cm}^2$, $g_{slow} = 20\text{mS/cm}^2$, $g_L = 2\text{mS/cm}^2$, $\phi = 0.15$, $\beta_m = -1.2\text{mV}$, $\gamma_m = 18\text{mV}$, and $\gamma_w = 10\text{mV}$. $C = 2\mu\text{F/cm}^2$ is the membrane capacitance. We chose the input current to be a periodic set of rectangular steps of period T_i , height I_0 and width $\tau = 0.5\text{ms}$. Studying the HH model, we learned that the topology of the global bifurcation diagram is only weakly dependent on shape details of individual pulses, provided they remain short compared to the time scale of the main resonance [13, 21]. The calculations are carried out within the fourth-order Runge-Kutta scheme with the time step of 0.001ms . Individual runs at fixed parameters were carried out for $1000T_i$. Since the variation of β_w is sufficient to alter the excitability type of the model, we study the effect of β_w on the dynamics at finite frequencies. Changes of other parameters, β_m , g_{fast} , g_{slow} , γ_m , and γ_w , may result in similar evolution of the neuron's dynamics [8].

Figure 1 shows the response diagram in the period-amplitude plane for $\beta_w = 0$. In the limit $I_0 = \text{const}$ this choice leads to type 1 excitability [8]. In Fig. 1

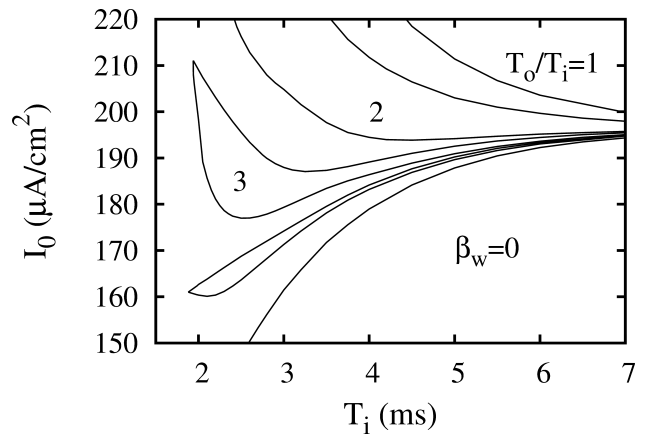


FIG. 1: Response diagram for $\beta_w = 0$. The main locked-in states are labeled by the inverse of the firing rate.

the dependence of the firing rate f_o/f_i on I_0 is continuous everywhere along the excitation threshold, scaling approximately as $(I_0 - I_{th})^{1/2}$, where I_{th} is the value of I_0 at the threshold.

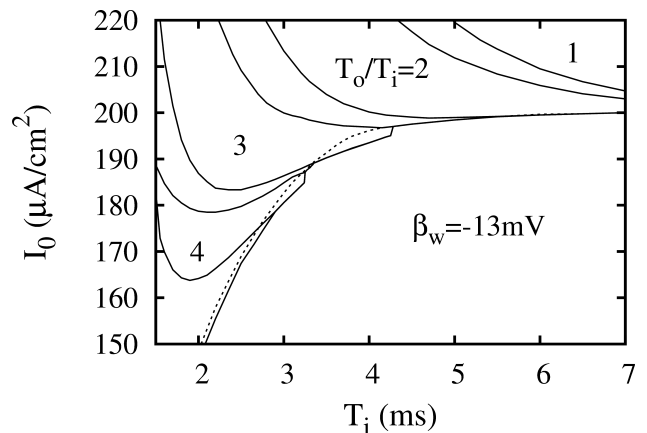


FIG. 2: Response diagram for $\beta_w = -13\text{mV}$. The locked-in states of order 3:1 and higher are bistable along the threshold. However the 2:1 state remains monostable. The dashed line separates the monostable regime from the bistable area. We have verified that MMT does not appear in this case.

When $\beta_w = -13\text{mV}$, the neuron displays class 2 dynamics for a constant current. In Fig. 2 we can see that the firing rate is a discontinuous function of the current amplitude also at high stimulation frequencies. For $T_i < 4\text{ms}$ almost the entire threshold is bistable. However, for $T_i > 4\text{ms}$ the system remains monostable. More precisely, the bistability does not extend beyond the 3:1 state and the edge of the 2:1 state is monostable. The low-frequency response in Figs. 1 and 2 is very similar. Wang et al. [22] also noted the similarity of response in this regime for a sinusoidal input.

Fig. 3 shows the response diagram for $\beta_w = -23\text{mV}$. There are now large bistable regions of the states 3:1 and 2:1. The high-frequency part of the diagram, for

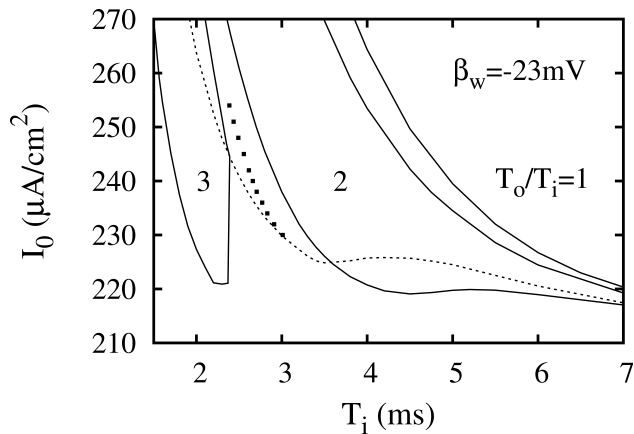


FIG. 3: Response diagram for $\beta_w = -23\text{mV}$. The dashed line separates the monostable regime from the bistable area. The location of the odd-all multimodal transition is denoted by full squares. For $1.5\text{ms} < T_i < 5\text{ms}$ this diagram closely resembles the one obtained for the HH model [13].

$T_i < 5\text{ms}$, closely resembles the regime of the HH model where the MMT occurs [15, 17]. We have analyzed the ISI histogram and found the same dynamic singularity in the ML model. The location of the transition is indicated in Fig. 3 by full squares. The f_o vs I_0 dependence in the interval between the MMT and the 2:1 state is approximately linear, as in the HH model [15]. The MMT along the T_i axis for $\beta_w = -23\text{mV}$ is shown in Fig. 4. The weight of even modes drops sharply in the vicinity of the minimum of the firing rate. The edges of individual modes near the transition scale logarithmically, as in the HH model [15]. All these signatures of the MMT and the topology of the bifurcation diagram in the vicinity of the MMT in the ML model are identical to the HH model. Therefore it is reasonable to conclude that (i) these may be universal properties associated with the MMT, and (ii) MMT occurs in many other type 2 or type 3 resonant neurons.

Fig. 5 shows sample $V(t)$ runs on both sides of the even-all transition. In the top panel, obtained at $T_i = 2.65\text{ms}$, the even modes 4:1 and 8:1 dominate. In the bottom panel obtained at $T_i = 2.45\text{ms}$ only odd modes are present. Here the height of the $V(t)$ peak correlates with the length of the preceding ISI. A careful examination of the peak heights reveals a preference for a $T_o = 3T_i$, following the action potential with the maximum value of V . This preference is manifested either as (i) another action potential, or as (ii) subthreshold peak with a height somewhat larger than that of its immediate neighbors. Judging by the height of subthreshold peaks there is a clear preference for a period $2T_i$ subthreshold oscillation. We can view the odd-only periods in the bottom panel as a sum of $3T_i + 2nT_i$, where $n = 0, 1, \dots$

We also analyzed the ISI histogram as a function of β_w , looking for signs of the MMT. For $\beta_w = -13\text{mV}$ we can see a precursor of the odd-all MMT in Fig. 6. There is a local minimum of f_o/f_i at $I_0 = 198.2\mu\text{A}/\text{cm}^2$ and

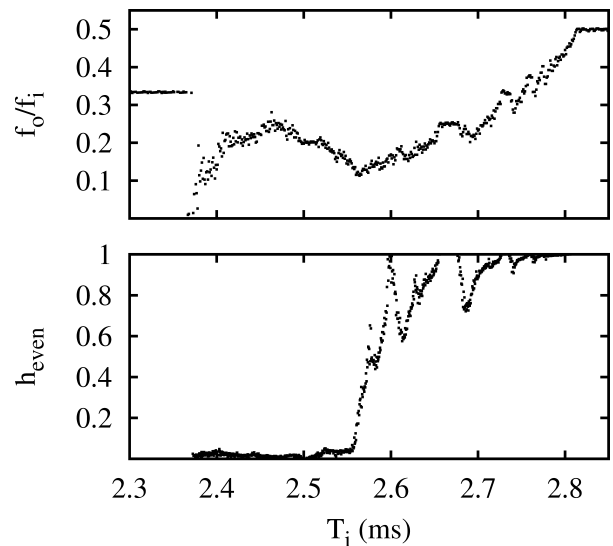


FIG. 4: The firing rate (top) and the weight of even modes (bottom) for $\beta_w = -23\text{mV}$ and $I_0 = 245\mu\text{A}/\text{cm}^2$.

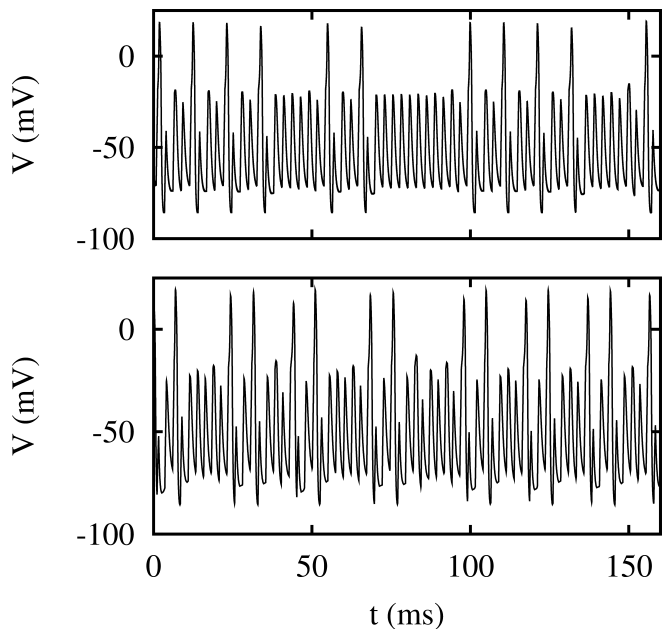


FIG. 5: Sample $V(t)$ run for $\beta_w = -23\text{mV}$, $I_0 = 245\mu\text{A}/\text{cm}^2$. The top panel contains data taken above the odd-all transition at $T = 2.65\text{ms}$. Here the even modes are more frequent than the odd ones but there is also some admixture of the odd modes. The bottom panel shows data at $T_i = 2.45\text{ms}$. Note the absence of even multiples of the driving period in the bottom panel. Here the response contains only the following multiples of T_i : 3, 5, 7, and 9.

a significant decrease of the participation rate of even modes close to the threshold.

The MMT is tied to the appearance of bistability along the bottom edge of the 2:1 state, which occurs for $\beta_w < -14.5\text{mV}$. In Fig. 7 we can see that for $\beta_w = -18\text{mV}$ the MMT is already well developed. As

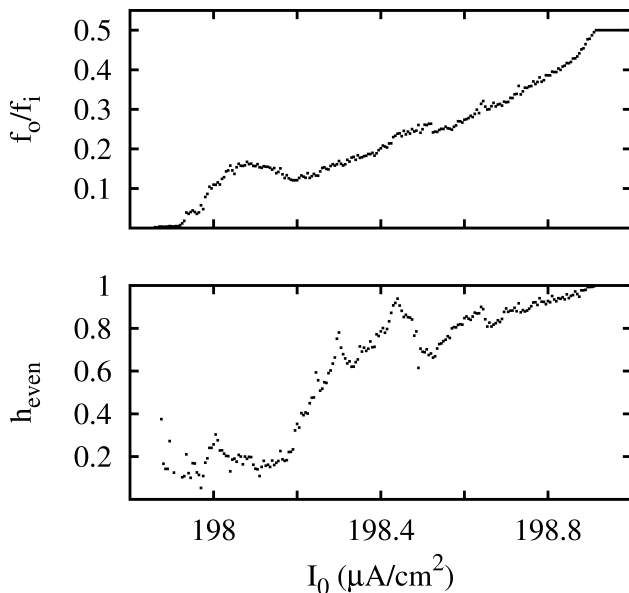


FIG. 6: The firing rate and the joint histogram weight of even modes for $\beta_w = -13\text{mV}$ and $T_i = 4.7\text{ms}$. A precursor of the multimodal transition can be seen near $I_0 = 198.2\mu\text{A}/\text{cm}^2$. There is a well pronounced local minimum of the f_o/f_i and a significant reduction of the participation rate of even modes.

the MMT is approached from above, only very high order even modes remain. The edges of the even modes scale logarithmically as a function of $|I_0 - I^*|$, where I^* is the current amplitude at which the transition occurs. When the bistability of the state 2:1 disappears near $\beta_w = -29\text{mV}$, so does the MMT. At this value of β_w the 3:1 state vanishes from the global bifurcation diagram.

III. CONCLUSIONS

The dynamics of neurons at frequencies above the resonant frequency is not directly related to either class 2 or class 3 excitability. The global bifurcation diagram of the class 3 ML model for $\beta_w = -23\text{mV}$ closely resembles the class 2 HH model [15] at intermediate frequencies. This is consistent with the remarks of Prescott et al. [8] that neurons should not be labeled as being strictly type 2 or type 3. The transition to bistability at the edge of a 2:1 state in a model stimulated by a train of current pulses does not occur for the same parameter values as the transition to bistability for a constant current. The bistability appears first in the limit of high frequency stimulation. As β_w decreases further, the perithreshold regions for larger T_i also become bistable. The MMT occurs when both the 2:1 and the 3:1 state have bistable regions along the threshold. The ability to predict the existence of the MMT from the topology of the locked-in states in the perithreshold regime is of course a very useful property. Testing for bistabilities near the threshold

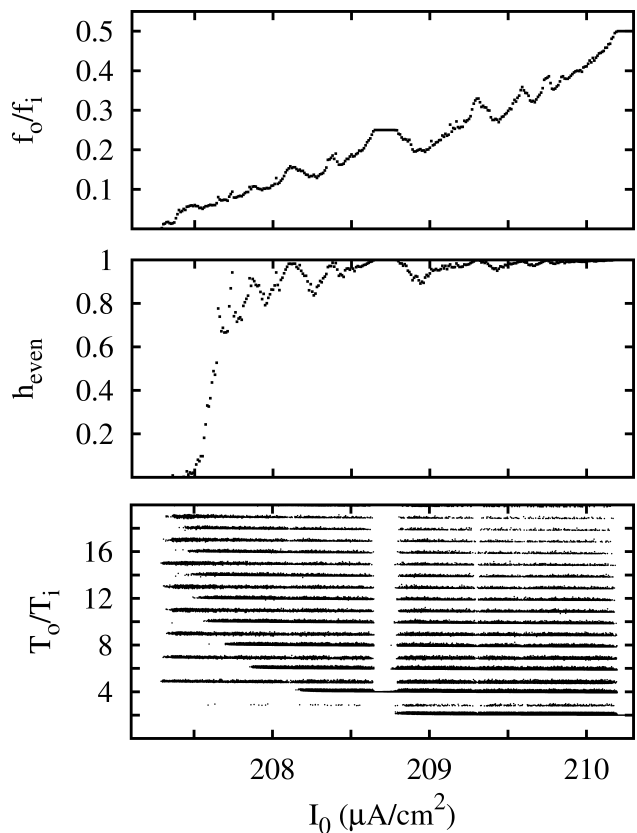


FIG. 7: From top to bottom: the firing rate, the joint histogram weight of even modes, and the ISI spectrum for $\beta_w = -18\text{mV}$ and $T_i = 3.7\text{ms}$. The multimodal transition occurs at $I_0 = 207.5\mu\text{A}/\text{cm}^2$.

is much simpler and computationally much more efficient than analyzing the evolution of the entire ISI histogram as a function of pulse frequency or amplitude.

Wang et al. [22] noted the similarity of class 1 and class 2 neuron response to sinusoidal signal at low frequencies. This is not surprising, once we note, that the threshold bistability, and a discontinuity of the f_o/f_i associated with it, appears first in the limit of high f_i and extends towards low f_i with decreasing β_w . When $\beta_w < -14.5\text{mV}$, the 3:1 state becomes bistable and the entire threshold at high frequencies rises significantly. The emergence of class 3 behavior may be viewed as a strong rigidity of neuron dynamics at high f_i .

We could also think of an alternative classification of neuron excitability for stimuli of finite frequency: (i) class 1, where the firing rate is a continuous function of I_0 everywhere along the threshold, (ii) class 2, with bistabilities at the edges of high-order locked-in states, (iii) class 3, where the MMT exists, and (iv) class 4, where both the MMT and the bistabilities are absent and the neuron responds to a constant current by emitting only a few spikes.

The presence of the MMT in both the ML and HH model suggests that the same transition is present in

other resonant neuron models classified as type 2 or type 3 cells. The existence of MMT may have important physiological consequences. It may be relevant in the high-frequency auditory nerve fiber stimulation [23] and possibly in the clinical procedure of deep brain stimulation [24].

Acknowledgments

Some of the computations were performed in the Computer Center of the Tri-city Academic Computer Network

in Gdansk.

References

-
- [1] A. L. Hodgkin, *J. Physiol. (London)* **107** 165 (1948).
 - [2] A. L. Hodgkin and A. F. Huxley, *J. Physiol. (London)* **117**, 500 (1952).
 - [3] T. Tateno, A. Harsch, and H. P. C. Robinson, *J. Neurophysiol.* **92**, 2283 (2004).
 - [4] T. Tateno and H. P. C. Robinson, *J. Neurophysiol.* **95**, 2650 (2006).
 - [5] C. Morris and H. Lecar, *Biophys. J.* **35**, 193 (1981).
 - [6] J. Rinzel and G. B. Ermentrout, In: C. Koch and I. Segev, eds. *Methods in Neuronal Modeling: from Ions to Networks*. Cambridge (Massachusetts): The MIT Press, pp. 251-291.
 - [7] J. L. Hindmarsh and R. M. Rose, *Proc. R. Soc. London B* **221**, 87 (1984).
 - [8] S. A. Prescott, Y. De Koninck, and T. J. Sejnowski, *PLoS Comput. Biol.* **4**, e1000198 (2008).
 - [9] S. A. Prescott, S. Ratte, Y. De Koninck, and T. J. Sejnowski, *J. Neurophysiol.* **100**, 3030 (2008).
 - [10] J. R. Clay, *J. Neurophysiol.* **80**, 903 (1998).
 - [11] J. R. Clay, *Prog. Biophys. Mol. Biol.* **88**, 59 (2005).
 - [12] J. R. Clay, D. Paydarfar, and D. B. Forger, *J. R. Soc. Interface* **5** 1421 (2008).
 - [13] L. S. Borkowski, *Phys. Rev. E* **83**, 051901 (2011).
 - [14] H. S. Strogatz, *Nonlinear Dynamics and Chaos*, Perseus (Cambridge, 1994).
 - [15] L. S. Borkowski, *Phys. Rev. E* **80**, 051914 (2009).
 - [16] N. Takahashi, Y. Hanyu, T. Musha, R. Kubo, and G. Matsumoto, *Physica D* **43**, 318 (1990).
 - [17] L. S. Borkowski, *Phys. Rev. E* **82**, 041909 (2010).
 - [18] M. St-Hilaire and A. Longtin *J. Comput. Neurosci.* **16** 299 (2004).
 - [19] R. Naud, N. Marcille, C. Clopath, and W. Gerstner, *Biol. Cybern.* **99** 335 (2008).
 - [20] M. A. D. Roa, M. Copelli, O. Kinouchi, and N. Caticha, *Phys. Rev. E* **75** 021911 (2007).
 - [21] L. S. Borkowski, arXiv.org:1105.5376 [physics.bio-ph].
 - [22] H. Wang, L. Wang, L. Yu, and Y. Chen, *Phys. Rev. E* **83**, 021915 (2011).
 - [23] D. E. O’Gorman, J. A. White, and C. A. Shera, *J. Assoc. Res. Otolaryngol.* **10**, 251 (2009).
 - [24] C. C. McIntyre and W. M. Grill, *Ann. Biomed. Eng.* **28**, 219 (2000).